PCCP

Physical Chemistry Chemical Physics

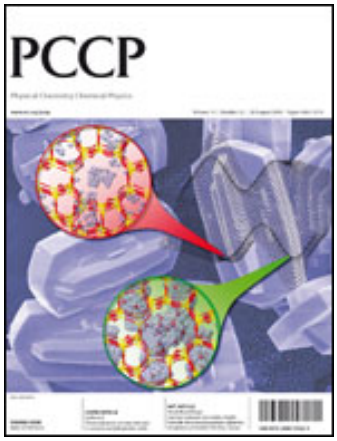

This paper is published as part of a PCCP Themed Issue on:

Water at interfaces

Guest Editor: Martin McCoustra

Editorial

Communications

Papers

Raman spectra of complexes of HNO_3 and NO_3^- with NO_2 at surfaces and with N_2O_4 in solution
Michael A. Kamboures, Wytze van der Veer, R. Benny Gerber and Leon F. Phillips, *Phys. Chem. Chem. Phys.*, 2008, **10**, 4748
DOI: 10.1039/b810081k

Molecular level structure of the liquid/liquid interface. Molecular dynamics simulation and ITIM analysis of the water-CCl_4 system
Lívia B. Pártay, George Horvai and Pál Jedlovszky, *Phys. Chem. Chem. Phys.*, 2008, **10**, 4754
DOI: 10.1039/b807299j

Solvent structures of mixed water/acetonitrile mixtures at chromatographic interfaces from computer simulations
Jörg Braun, Antony Fouqueau, Raymond J. Bemish and Markus Meuwly, *Phys. Chem. Chem. Phys.*, 2008, **10**, 4765
DOI: 10.1039/b807492e

Ion spatial distributions at the liquid–vapor interface of aqueous potassium fluoride solutions
Matthew A. Brown, Raffaella D'Auria, I.-F. William Kuo, Maria J. Krisch, David E. Starr, Hendrik Bluhm, Douglas J. Tobias and John C. Hemminger, *Phys. Chem. Chem. Phys.*, 2008, **10**, 4778
DOI: 10.1039/b807041e

Trapping proton transfer intermediates in the disordered hydrogen-bonded network of cryogenic hydrofluoric acid solutions
Patrick Ayotte, Sylvain Plessis and Patrick Marchand, *Phys. Chem. Chem. Phys.*, 2008, **10**, 4785
DOI: 10.1039/b806654j

Aqueous divalent metal–nitrate interactions: hydration *versus* ion pairing
Man Xu, James P. Larentzos, Mazen Roshdy, Louise J. Criscenti and Heather C. Allen, *Phys. Chem. Chem. Phys.*, 2008, **10**, 4793
DOI: 10.1039/b807090n

Structure and dynamics of water at a clay surface from molecular dynamics simulation
Virginie Marry, Benjamin Rotenberg and Pierre Turq, *Phys. Chem. Chem. Phys.*, 2008, **10**, 4802
DOI: 10.1039/b807288d

Proton mobility in thin ice films: a revisit
Eui-Seong Moon, Chang-Woo Lee and Heon Kang, *Phys. Chem. Chem. Phys.*, 2008, **10**, 4814
DOI: 10.1039/b807730b

Thermodynamics of water intrusion in nanoporous hydrophobic solids
Fabien Cailliez, Mickael Trzpit, Michel Soulard, Isabelle Demachy, Anne Boutin, Joël Patarin and Alain H. Fuchs, *Phys. Chem. Chem. Phys.*, 2008, **10**, 4817
DOI: 10.1039/b807471b

Gas phase hydration of organic ions
Paul O. Momoh and M. Samy El-Shall, *Phys. Chem. Chem. Phys.*, 2008, **10**, 4827
DOI: 10.1039/b809440n

Water photodissociation in free ice nanoparticles at 243 nm and 193 nm
Viktoriya Poterya, Michal Fárník, Milan Ončák and Petr Slavíček, *Phys. Chem. Chem. Phys.*, 2008, **10**, 4835
DOI: 10.1039/b806865h

Electroacoustic and ultrasonic attenuation measurements of droplet size and ζ-potential of alkane-in-water emulsions: effects of oil solubility and composition
Alex M. Djerdjev and James K. Beattie, *Phys. Chem. Chem. Phys.*, 2008, **10**, 4843
DOI: 10.1039/b807623e

Gas hydrate nucleation and cage formation at a water/methane interface
Robert W. Hawtin, David Quigley and P. Mark Rodger, *Phys. Chem. Chem. Phys.*, 2008, **10**, 4853
DOI: 10.1039/b807455k

Hydration water rotational motion as a source of configurational entropy driving protein dynamics. Crossovers at 150 and 220 K
J.-M. Zanotti, G. Gibrat and M.-C. Bellissent-Funel, *Phys. Chem. Chem. Phys.*, 2008, **10**, 4865
DOI: 10.1039/b808217k

Influence of wettability and surface charge on the interaction between an aqueous electrolyte solution and a solid surface
Svetlana Guriyanova and Elmar Bonaccurso, *Phys. Chem. Chem. Phys.*, 2008, **10**, 4871
DOI: 10.1039/b806236f

Molecular dynamics study of hydrated imogolite 2. Structure and dynamics of confined water
Benoît Creton, Daniel Bougeard, Konstantin S. Smirnov, Jean Guilment and Olivier Poncelet, *Phys. Chem. Chem. Phys.*, 2008, **10**, 4879
DOI: 10.1039/b803479f

Assessing the performance of implicit solvation models at a nucleic acid surface
Feng Dong, Jason A. Wagoner and Nathan A. Baker, *Phys. Chem. Chem. Phys.*, 2008, **10**, 4889
DOI: 10.1039/b807384h

Aqueous peptides as experimental models for hydration water dynamics near protein surfaces
Cecile Malardier-Jugroot, Margaret E. Johnson, Rajesh K. Murarka and Teresa Head-Gordon, *Phys. Chem. Chem. Phys.*, 2008, **10**, 4903
DOI: 10.1039/b806995f

Melting behavior of water in cylindrical pores: carbon nanotubes and silica glasses
M. Sliwinska-Bartkowiak, M. Jazdzewska, L. L. Huang and K. E. Gubbins, *Phys. Chem. Chem. Phys.*, 2008, **10**, 4909
DOI: 10.1039/b808246d

Increased interfacial thickness of the NaF, NaCl and NaBr salt aqueous solutions probed with non-resonant surface second harmonic generation (SHG)
Hong-tao Bian, Ran-ran Feng, Yan-yan Xu, Yuan Guo and Hong-fei Wang, *Phys. Chem. Chem. Phys.*, 2008, **10**, 4920
DOI: 10.1039/b806362a

Determination of the electron's solvation site on D_2O/Cu(111) using Xe overlayers and femtosecond photoelectron spectroscopy
Michael Meyer, Julia Stähler, Daniela O. Kusmierek, Martin Wolf and Uwe Bovensiepen, *Phys. Chem. Chem. Phys.*, 2008, **10**, 4932
DOI: 10.1039/b807314g

Breakdown of hydration repulsion between charged surfaces in aqueous Cs^+ solutions
Ronit Goldberg, Liraz Chai, Susan Perkin, Nir Kampf and Jacob Klein, *Phys. Chem. Chem. Phys.*, 2008, **10**, 4939
DOI: 10.1039/b807459n

A macroscopic water structure based model for describing charging phenomena at inert hydrophobic surfaces in aqueous electrolyte solutions
Johannes Lützenkirchen, Tajana Preočanin and Nikola Kallay, *Phys. Chem. Chem. Phys.*, 2008, **10**, 4946
DOI: 10.1039/b807395c

Thermally induced mixing of water dominated interstellar ices
Daren J. Burke, Angela J. Wolff, John L. Edridge and Wendy A. Brown, *Phys. Chem. Chem. Phys.*, 2008, **10**, 4956
DOI: 10.1039/b807220e

Water hydrogen bond analysis on hydrophilic and hydrophobic biomolecule sites
Daniela Russo, Jacques Ollivier and José Teixeira, *Phys. Chem. Chem. Phys.*, 2008, **10**, 4968
DOI: 10.1039/b807551b

Hydronium and hydroxide at the interface between water and hydrophobic media
Robert Vácha, Dominik Horinek, Max L. Berkowitz and Pavel Jungwirth, *Phys. Chem. Chem. Phys.*, 2008, **10**, 4975
DOI: 10.1039/b806432f

Average molecular orientations in the adsorbed water layers on silicon oxide in ambient conditions
Anna L. Barnette, David B. Asay and Seong H. Kim, *Phys. Chem. Chem. Phys.*, 2008, **10**, 4981
DOI: 10.1039/b810309g

Interfacial water structure at polymer gel/quartz interfaces investigated by sum frequency generation spectroscopy
Hidenori Noguchi, Minowa Hiroshi, Taiki Tominaga, Jian Ping Gong, Yoshihito Osada and Kohei Uosaki, *Phys. Chem. Chem. Phys.*, 2008, **10**, 4987
DOI: 10.1039/b807297n

Co-adsorption of water and hydrogen on Ni(111)
Junjun Shan, Jacques F. M. Aarts, Aart W. Kleyn and Ludo B. F. Juurlink, *Phys. Chem. Chem. Phys.*, 2008, **10**, 4994
DOI: 10.1039/b808219g

Water–methanol mixtures: topology of hydrogen bonded network
Imre Bakó, Tünde Megyes, Szabolcs Bálint, Tamás Grósz and Viorel Chihaia, *Phys. Chem. Chem. Phys.*, 2008, **10**, 5004
DOI: 10.1039/b808326f

Photochemistry of ethyl chloride caged in amorphous solid water†

Yousif Ayoub and Micha Asscher*

Received 7th May 2008, Accepted 21st July 2008
First published as an Advance Article on the web 23rd September 2008
DOI: 10.1039/b807803n

Caging and photo-induced decomposition of ethyl chloride molecules (EC) within a layer of amorphous solid water (ASW) on top of clean and oxygen-covered Ru(001) under ultra-high vacuum (UHV) conditions are presented. The caged molecules were estimated to reside 1.5 ± 0.2 nm above the solid surface, based on parent molecule thermal decomposition on the clean ruthenium. Dissociative electron attachment (DEA) of the caged molecules following 193 nm laser irradiation, result in initial fragmentation to ethyl radical and chloride anion. It was found that photoreactivity on top of the clean ruthenium surface (Ru) is twenty times faster than on the oxygen-covered surface (O/Ru), with DEA cross sections: $\sigma_{Ru} = (3.8 \pm 1) \times 10^{-19}$ cm^2 and $\sigma_{O/Ru} = (2.1 \pm 0.3) \times 10^{-20}$ cm^2. This difference is attributed to the higher work function of oxygen-covered ruthenium, leading to smaller electron attachment probability due to mismatch of the ruthenium photo-electron energy with the adsorbed EC excited electron affinity levels. EC molecules fragmented within the cage, result in post-irradiation TPD spectra that reveal primarily C_4H_8, C_3H_5 and C_3H_3, without any oxygen-containing molecules. Unique stabilization of the photoproducts has been observed with the first layer of water molecules in direct contact with the substrate, desorbing near 180 K, a significantly higher temperature than the desorption of fully caged molecules. This study may contribute for understanding stratospheric photochemistry and processes in interstellar space.

1. Introduction

Photo-induced chemistry of molecules interacting with solid interfaces has been the focus of interest and intensive research in recent years.[1–3]. Early[3] and more recent studies[4] have discussed photodesorption mechanisms from oxide surfaces and ices respectively. A stabilizing effect of the ice environment was reported for the case of trapped polycyclic aromatic hydrocarbon (PAHs) ions, formed by ionizing irradiation, attempting to mimic conditions at interstellar space, based on IR laboratory studies.[5,6a] The same detection technique has also been employed to monitor long-chain hydrocarbons, formed following UV irradiation of ice analogs made of formaldehyde and methanol.[6b] Other mechanisms to form interstellar hydrocarbons were reviewed in ref. 6*c*.

Photo-induced reactivity on top of solid surfaces has become increasingly important in recent years within the context of photocatalysis, mostly with oxides (*e.g.* TiO_2) as catalysts at ambient conditions.[7] Under these conditions, molecules often interact with the solid surfaces in the presence of a few water layers. Understanding the role of neighbor water molecules that are not directly involved in the primary photo-event is therefore important.

Institute of Chemistry, The Hebrew University of Jerusalem, Jerusalem, Israel. E-mail: asscher@fh.huji.ac.il; Fax: +972 (0)2 6525037; Tel: +972 (0)2 6585742

† This article was submitted as part of a Themed Issue on water at interfaces. Other papers on this topic can be found in issue 32 of vol. 10 (2008). This issue can be found from the *PCCP* homepage [http://www.rsc.org/pccp].

A central photodissociation pathway of adsorbed molecules on metallic and oxide surfaces involves dissociative (photo)-electron attachment mechanism.[1,2]

Caging of adsorbed molecules within water ice layers on well-defined metallic substrates has been observed already more than a decade ago. The first experimental demonstration of a molecular cage in amorphous solid water (ASW) was that of N_2,[8] while other studies have focused mostly on halogenated molecules, such as CCl_4,[9] CD_3Cl,[10] CD_3Br, but also other molecules were shown to be trapped by ASW, *e.g.* CO_2.[11] Subsequent desorption of the trapped molecules proceeds *via* an explosive, "volcano" mechanism.[8,9] Irradiation of molecular traps of this kind by UV light has been suggested as a possible origin, *via* photodesorption[12] and fragmentation of the trapped molecular species[13,14] of organic molecules in interstellar space.

In this report we describe the caging and subsequent photochemistry of ethyl chloride (EC) molecules, used as model for the study of halogenated hydrocarbon molecules in the stratosphere.[15] Quantifying the reactivity of caged molecules may potentially assist studies of photo-induced processes at interstellar space as well. The EC molecules were caged within layers of ASW on well-characterized Ru(001) and O/Ru(001) substrates under ultra-high vacuum (UHV) conditions. Subsequently the system was irradiated by 6.4 eV photons from an excimer laser. The clean and oxygen-covered ruthenium substrates were chosen to demonstrate substrate effects on photoreactivity over solid surfaces, often a neglected subject.

Several stable gaseous molecules are obtained following reactivity among the nascent photoproducts. Cross sections for these processes are reported.

2. Experimental

The experiments described in this report were performed in an ultra-high vacuum (UHV) apparatus, typical base pressure of 2×10^{-10} Torr, described elsewhere in detail.[13,16] The chamber is equipped with a quadrupole mass-spectrometer (QMS) that is covered by a glass tube with a 3 mm aperture in front, thus avoiding a record of desorption from surfaces other than the sample while improving sensitivity and selectivity. In addition to standard temperature-programmed desorption ΔP-TPD (P for pressure), average adsorbates dipole moment could be determined by means of a Kelvin probe, operated in a $\Delta\varphi$-TPD (φ for work function) mode as explained elsewhere.[16]

In addition, a mini excimer laser (PSX-100) provides 2.5 ns long pulses at 193 nm, 3 mJ per pulse, and variable repetition rate up to 100 Hz for the photo-excitation studies. The analysis of the photoproducts was based on post irradiation ΔP-TPD, simultaneously scanning a full range of masses (see Fig. 2 below) at a heating rate of up to 2 K s^{-1}. The Ru(001) sample, oriented to within 0.5 degrees of the (001) plane, could be cooled down to 82 K by pumping over a liquid nitrogen reservoir. Temperature was determined by a C-type thermocouple (W5%Re/W26%Re) and controlled to within 0.5 degrees using an ac resistive heating LabView routine.

3. Results and discussion

We have studied the photochemistry of EC molecules caged inside 25 bilayers (BL) ASW following 193 nm laser irradiation on clean Ru(001). An important element in this study was the potential effect of the underlying substrate. Therefore, we have compared results obtained from clean Ru(001) to the photo-activity on top of ordered oxygen-covered ruthenium, (2×1)–O/Ru(001). These substrates were chosen to focus on the substrate effect on the outcome of photo-induced processes rather than attempting to mimic actual surfaces in the stratosphere or in interstellar space.

Before discussing the photochemistry within the cage it is important to briefly introduce the procedure used to form a molecular cage under ASW.

3.1 Cage formation: EC@ASW

The cage formation mechanism for EC is practically identical to the first molecular cage observed with N_2 (see ref. 8) and other molecules in subsequent studies.[9–11]

Water layers were grown by back-filling the vacuum chamber, determining the actual exposure and layer thickness based on post-exposure-uptake TPD measurements. Such deposition conditions form compact amorphous solid water, as was shown before.[17] The co-adsorption of EC molecules with a gradually denser coverage of water leads to compression of the EC molecules on the surface.[10] At thick ASW layers [more than 20 BL, where 1 BL = $(1 \pm 0.1) \times 10^{15}$ molecules cm^{-2} on Ru(001)][18,19] a cage has fully been developed, as evidenced by an extremely narrow, explosive TPD peak with a typical width of 2–3 degrees at half maximum, near the onset desorption of ASW at 165 K.

A fixed EC coverage of 0.3 ML was deposited first at 82 K, followed by gradually thicker layers of ASW. The EC TPD signal (mass 64) reveals three important stages of the cage formation. Desorption of EC without water co-adsorption (Fig. 1A) is characterized by a broad desorption peak, centered at 175 K. At ASW converge of 6 BL one can distinguish two different populations. The peak at 125 K originates from a fraction of EC molecules that were "floating" on top of the ASW layer, as understood from the low temperature desorption, before any water desorption takes place. These molecules have no direct contact with the substrate. In order to verify that these molecules are on top of the water layer, 0.3 ML EC were deposited directly on top of a 6 BL thick ASW layer. The subsequent TPD is shown as a dashed line in Fig. 1B, revealing identical behavior with the floating molecules. The binding energy of EC to water was estimated based on standard Redhead TPD lineshape analysis of Fig. 1B, assuming a pre-exponential factor of 10^{13} s^{-1} for the first order desorption rate. Activation energy for desorption and its uncertainty, as derived from the TPD analysis, is 8.4 ± 1 kcal mol^{-1}. This is a rather similar result to the strength of interaction among EC molecules, derived similarly from the TPD of multilayer of EC molecules (not shown), which is 8.1 ± 1 kcal mol^{-1}.

A new and gradually narrowing peak emerges near 165 K, at the onset of ASW desorption. This peak of caged EC molecules contains most of the molecules that were previously residing on the metallic substrate. There are parent molecules and photochemically formed molecules that tend to be associated with and stabilized by water molecules of the first layer, desorbing at 178 K.

An important question that has not yet been addressed regarding the caging process of molecules under layers of ASW, is the location or distance of the trapped molecules from the substrate, after the caging process has been completed, as shown *via* TPD in Fig. 1C.

We have previously demonstrated, in the case of CD_3Cl trapped in ASW,[10] based on work function change measurements, that the caged molecules were lifted upwards, away from the surface by the nature of interaction with the post-adsorbed water molecules on a clean Ru(001) surface.

In order to better define the position of the EC molecules above the substrate while caged within ASW, we took advantage of the fact that a fraction of the first monolayer of parent EC molecules (about 0.2) undergoes dissociation upon thermal heating during TPD on the clean Ru(001). This dissociation is manifested by the uptake of hydrogen molecules desorbing at 350 K, as a result of further dissociation and dehydrogenation of the ethyl fragment.

No hydrogen signal could be detected from a full cage as seen in Fig. 1C on top of clean Ru(001). This observation indicates, we predict, that the caged molecules are too far from the surface, therefore do not reach it upon cage explosive desorption.

In order to clarify this assumption, we have defined a maximum distance for EC molecules to reach the metallic surface during desorption and leave its hydrogen desorption signature. The calibration approach has been to mimic the cage by constructing a sandwich of EC molecules between two films of ASW. A variable thickness first layer attached to the ruthenium substrate, then a fixed 0.3 ML of EC on top and

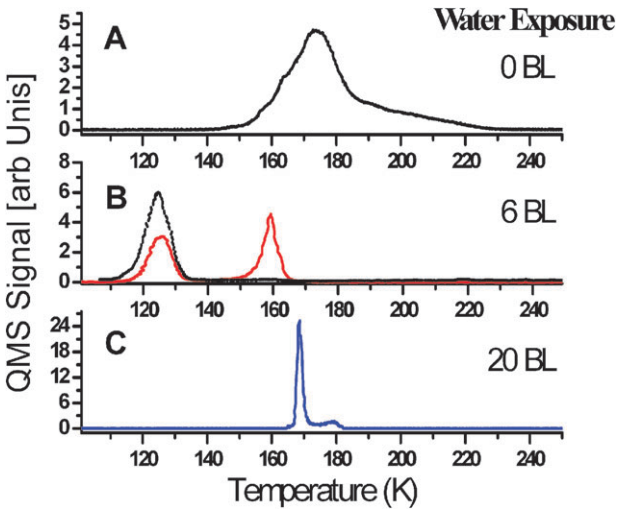

Fig. 1 ΔP-TPD at mass 64 (parent EC molecule) following water post-deposition on top of a fixed 0.3 ML EC on clean Ru(001). The TPD spectra demonstrate the gradual (from A to B) compression and eventual full caging (C) of EC under the indicated ASW layers. Note the substantially higher but narrower peak recorded following complete caging under 20 BL. The dashed line in (B) was obtained from 0.3 ML EC directly deposited on top of a 6 BL thick water layer.

then a second, constant thickness (10 BL) layer of ASW. The details of this study will appear elsewhere, but the summary of this test has been that at layer thickness of 9 ± 1 BL and above, the EC molecules do not reach the bottom ruthenium substrate during the desorption of this sandwich composition.

We conclude that the caged molecules must reside within a distance of at least 1.5 ± 0.2 nm from the surface.

3.2 Photochemistry of caged EC

Once the EC@ASW cage has been established, it was irradiated by UV light at 193 nm, photon energy of 6.4 eV, at a fixed pulse energy of 3 ± 0.5 mJ per pulse. At this pulse energy, the estimated thermal heating of the ruthenium substrate was less than 8 K above the substrate temperature of 82 K,[20] which eliminates any thermal effects due to the UV laser irradiation.

Parent EC molecules caged in a matrix of ASW cannot undergo photodesorption. On the other hand, photofragments formed within the cage may react with each other but potentially also with the host water molecules surrounding the cage. An additional experimental benefit is gained from the fact that the parent molecules as well as the various photoproducts are all explosively desorbing at the same temperature range near 165 K, the onset of ASW desorption (evidenced by the dark blue–green stripe at that temperature scale in Fig. 2).

We have developed a way to simultaneously scan a complete mass range during a single TPD run. This multimass-scan is an efficient mode of operation, particularly for an initial screening of new products that have not yet been identified.

A scan of this kind is demonstrated in a 3D form, where QMS signal is displayed *vs.* mass and temperature, as shown in Fig. 2. Fig. 2B was obtained following EC cage irradiation for 90 sec (equivalent to photons dose of 5.2×10^{18} at 193 nm), while in Fig. 2A the same plot is a thermal scan of caged EC molecules, without irradiation.

Post-irradiation stable molecular products can be observed in the TPD scan at the mass range of 54–57 a.u. and 39–43 a.u., shown in the blow-up in Fig. 2B.

There is significant background signal at masses 35 and 37 due to chlorine, a dissociation product inside the QMS that masks other possible stable molecular products at the same mass range. It is evident from analysis of Fig. 2 that most of the cage molecular content, including the parent molecules and the photoproducts, explosively desorb simultaneously at 165 K upon the onset of ice desorption. Yet, a significant fraction of the molecules are stabilized by water molecules in the first layer, therefore desorbing only near 178 K.

Post-irradiation TPD spectra in Fig. 3 reveal the EC parent molecule (mass 64) uptake as a function of irradiation time on clean Ru (Fig. 3A) and O/Ru (Fig. 3B) substrates. The total EC uptake signal decreases monotonically at a first order-like kinetics with photons exposure.

The comparison between photo-induced decomposition on clean *vs.* oxygen-covered ruthenium surfaces originates from the attempt to modify the strength of interaction between photo-excited, negatively charged EC (dissociative electron attachment process—DEA[1,2]) with the underlying substrate. Generally one expects that the oxygen-covered surface, on top

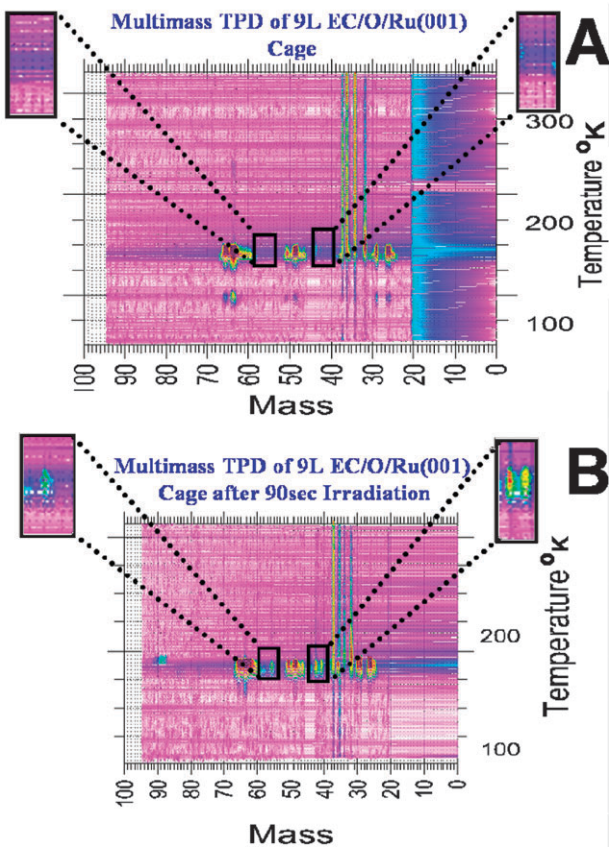

Fig. 2 (A) A multimass-TPD taken simultaneously at all masses between 20–95 a.u. in a 3D representation without irradiation and (B) following 90 s of irradiation time (equivalent to 5.2×10^{18} 193 nm photons). The blow-up reveals the signal of various photoproducts of the EC@ice system.

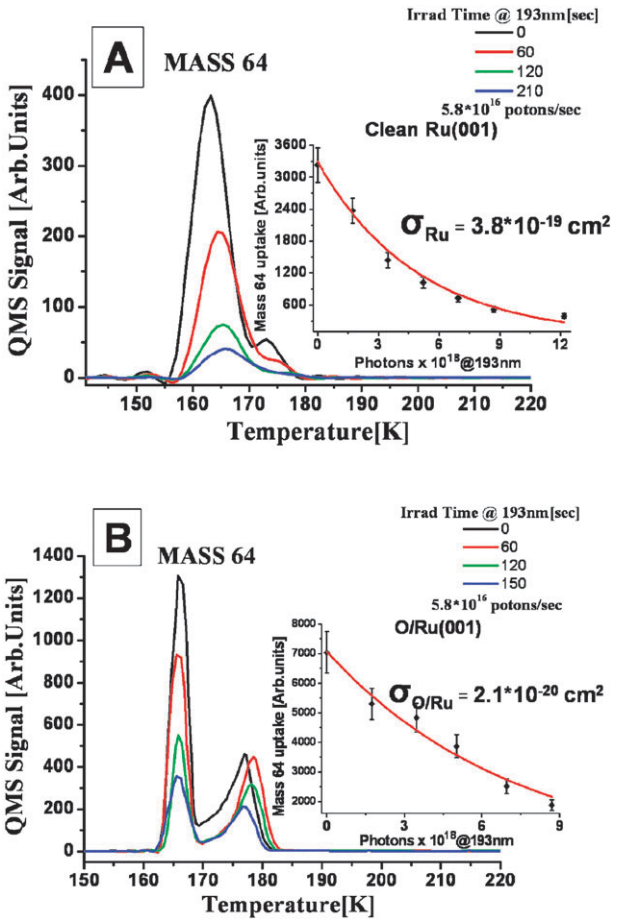

Fig. 3 (A) ΔP-TPD spectra of 0.3 ML EC (64 a.u.) on clean Ru and (B) O/Ru substrate following 0, 60, 120 and 150 s exposure to a 193 nm photon flux of 5.8×10^{16} photons s^{-1}. The insets reveal the decomposition rate of the parent molecule *via* uptake QMS signal at mass 64 as a function of irradiation time. The resulting cross section is shown for both substrates. Heating rate is 2 K s^{-1}.

of which the parent molecule does not thermally dissociate, will couple less strongly also to the excited EC.

A similar behavior is well known in the case of thin oxide films (*e.g.* photodesorption of NO[21] and CO[3] from NiO/Ni, on top of which overall photoreactivity is significantly larger than on the clean metals).

Contrary to the above discussion, the cross section for photo-induced decomposition of the caged EC molecules is smaller by a factor of twenty on the (2×1)–O/Ru(001) substrate ($\sigma_{O/Ru} = (2.1 \pm 0.3) \times 10^{-20}$ cm^2) compared with the clean Ru ($\sigma_{Ru} = (3.8 \pm 1) \times 10^{-19}$ cm^2). The cross section is extracted from the expression $I_{(t)} = I_{(0)}e^{-\sigma Ft}$ (see discussion *e.g.* in ref. 21 and 22), where $I_{(t)}$ is the QMS signal, and F is the photon flux, the uncertainty represents two standards of deviation as extracted from the fit to the decay curves in Fig. 3A and B. The caged molecules in the present study differ from previous photoreactivity studies of molecules adsorbed in direct contact with a substrate in their distance from the surface. As discussed above, the EC molecules are trapped within the ASW film at least 1.5 nm away from the surface. Therefore the strength of interaction and therefore the quenching probability of the excited (negatively charged) EC is expected to be small and less sensitive to the variation between the clean metal and the oxygen-covered ruthenium. The overall probability for photoreactivity p_{tot} is the product of electron attachment (excitation) probability p_{att} and probability for quenching of the excited state (p_{quench}) that is the sum of all possible pathways. The two main competing de-excitation pathways are simple quenching in which the energy of the excited state is damped back to the bulk substrate (heating it) and the reactive channel of decomposition. Because of the large distance of the caged molecules, the quenching is not expected to be significantly different for the clean ruthenium metal and the oxygen-covered surface. The twenty-fold difference in the cross-section shown in Fig. 3 should therefore be attributed to the attachment process. A possible origin for this difference in attachment cross section between the bare metal and the oxygen-covered one, is the 1.2 eV higher work function of the O/Ru(001) compared to clean Ru(001).[23] The lower energy position of the Fermi level relative to the vacuum level in the O/Ru substrate, leads to excitation by the 6.4 eV photons to energy range that apparently does not overlap well the relevant excitation level of the caged EC molecule. We conclude that as a result, the probability for electron attachment in the O/Ru sample is about an order of magnitude smaller than that on the clean ruthenium sample, resulting in the overall smaller decomposition rate of the parent molecule: $\sigma_{Ru} \approx 20\ \sigma_{O/Ru}$. This significant sensitivity to the underlying substrate undermines the importance of direct photon absorption by the caged EC molecules.

Subsequent to parent molecules dissociation, fragments may react with each other and potentially also with the surrounding water molecules.[13] One should not expect identical behavior to occur on solid particles in the stratosphere or grains in interstellar space, because of the different chemical composition and electronic structure of these solid particles. However, more energetic vacuum UV photons (VUV), abundant in interstellar space, may lead to similar reactivity of caged molecules, a possible route for the formation of hydrocarbon species.[6]

The initial stage following DEA process includes photofragmentation of the parent EC molecule to the alkyl radical (C_2H_5) and to chloride anion. This fragmentation leads to the chemistry and new products we observed.

In Fig. 4, the most abundant photoproducts as a result of irradiation at 193 nm with photon energy of 6.4 ev are shown, at masses 39, 41 and 56. As mentioned before, possible products in mass range of 35–37 cannot be identified in our study due to large chlorine background signal. Post-irradiation TPD results in molecular products desorbing as caged molecules. However, for the relatively small density of products compared to the parent molecules, the higher temperature desorption peak near 178 K is the dominant TPD peak over the cage desorption at 165 K. This result is in contrast to the behavior of the caged parent molecule, where most of the TPD peak is the caged, explosive one near 165 K. Moreover, it is also rather different from previous results obtained following the photolysis of caged CD_3Cl, where the larger fraction of photoproducts has desorbed at 165 K.[13]

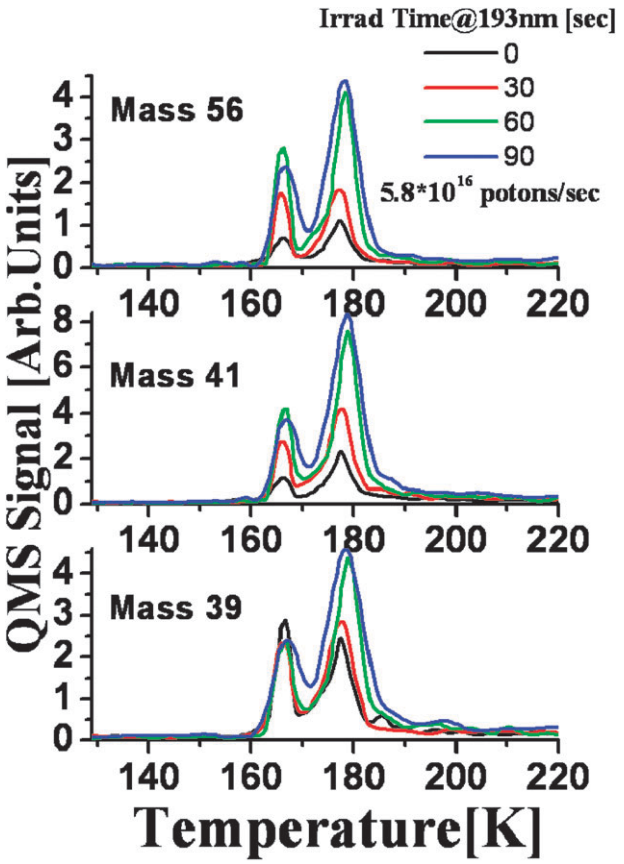

Fig. 4 ΔP-TPD spectra of photoproducts at masses 39, 41 and 56 following excitation of 0.3 ML of caged EC@ASW on O/Ru. Irradiation by 193 nm photons at a flux of 5.8×10^{16} cm^2 for the indicated exposure time.

The practical absence of any oxygen containing products suggests that unlike the methyl chloride case reported previously, the slightly longer hydrocarbon chain leads to preferred inter-alkyl chain interactions, that result in the formation of hydrocarbons such as butylene (C_4H_8, mass 56) and C_3H_5 (mass 41).

We conclude, therefore, that there is a stronger attraction and better stability of these hydrocarbon chains while attached to water molecules in direct bonding to the O/Ru surface (first layer) than as a "floating" cage within the ASW matrix.

We have noted that while forming these stable products, at irradiation times longer than 90 s, equivalent to a doze of more than 5.2×10^{18} photons, the products undergo fragmentation by the same UV light and their yield starts to decrease. The initial QMS signal growth *vs.* photon dosage can be translated into formation cross sections:

σ(mass 56) = $(9.3 \pm 1.5) \times 10^{-22}$ cm^2, σ(mass 41) = $(9.4 \pm 1.5) \times 10^{-22}$ cm^2, σ(mass 39) = $(8.2 \pm 1.5) \times 10^{-22}$ cm^2, on the 0.5 ML oxygen pre-covered Ru(001).

Beyond the above exposure to the UV light, photoproducts integrated desorption peaks start decreasing with photon dosage at higher cross sections:

σ(mass 56) = $(1.8 \pm 0.7) \times 10^{-20}$ cm^2, σ(mass 41) = $(1.7 \pm 0.7) \times 10^{-20}$ cm^2 and σ(mass 39) = $(2.4 \pm 0.7) \times 10^{-20}$ cm^2.

The photoproducts on the clean Ru surface undergo the same process except the fact that the turning point occurs already at smaller photon dosage, after 30 s (equivalent to 1.74×10^{18} 193 nm photons) of irradiation. This observation suggests a faster and more efficient decomposition of the photoproducts on the clean ruthenium, making it practically impossible to measure formation cross sections. The photo-decomposition process on the clean ruthenium, has indeed higher cross sections: σ(mass 56) = $(8.6 \pm 1.5) \times 10^{-19}$ cm^2, σ(mass 41) = $(4.6 \pm 1.5) \times 10^{-19}$ cm^2 and σ(mass 39) = $(3.4 \pm 1.2) \times 10^{-19}$ cm^2.

The most abundant product is found at mass 41 $\pm$ 1 a.u. (C_3H_5), presumably a direct reaction of "hot" ethyl with "hot" methyl. Ethyl is a direct fragment of the parent molecule while the methyl may be obtained from direct photodecomposition or DEA process of the ethyl radical.

A reaction between two ethyl radicals results in longer chain alkyl at mass 56 $\pm$ 1 (C_4H_8), with one double bond (butylene). Mass 39 $\pm$ 1 seems to be formed *via* a dehydrogenation of the photoproduct at mass 41 leading to (C_3H_4).

4. Conclusions

We have demonstrated the caging and subsequent photo-induced reactivity of ethyl chloride molecules within a layer of amorphous solid water on top of clean and oxygen-covered Ru(001). It was shown that the caged molecules reside 1.5 $\pm$ 0.2 nm above the solid surface. The photoreactivity is due to irradiation with an excimer laser at 193 nm, resulting in dissociative electron attachment (DEA) of the caged molecules. We have demonstrated that counterintuitively, the photoreactivity on top of the clean ruthenium surface is almost twenty times faster than on the oxygen-covered surface, with dissociation cross sections: $\sigma_{Ru} = 3.8 \times 10^{-19}$ cm^2 and $\sigma_{O/Ru} = 2.1 \times 10^{-20}$ cm^2. This difference is attributed to the higher work function of oxygen-covered ruthenium, resulting in a smaller electron attachment probability due to mismatch of the ruthenium photo-electron energy with the adsorbed EC excited electron affinity levels.

EC molecules decomposing within the cage result in photo-products with short-chain hydrocarbons but do not include oxygen-containing molecules which could have been obtained from a reaction with the surrounding water molecules. The most abundant products (C_4H_8, C_3H_5 and C_3H_3) are thought to be formed due to further fragmentation of the original ethyl radical by the subsequent pulses and strong hydrophobic interactions that prevent reactions of the hydrocarbon fragments with the surrounding water. Finally, unique stabilization of the photoproducts has been observed with the first layer of water molecules in direct contact with the substrate desorbing near 180 K, a significantly higher temperature than the typical desorption of caged molecules.

Molecular cations formed *via* high-energy photons (VUV) were reported to be stabilized by the water-ice matrix, representing interstellar photochemistry on grains. The present results of EC@ice reveal stabilization within the ice cage as well, but here fragments are either neutral (hydrocarbon radicals) or negative ions (chloride). The neutral radicals may facilitate the formation of longer-chain hydrocarbons.

This study has demonstrated the photo-induced formation of hydrocarbons. These results are potentially relevant to photoreactivity over solid particles in the stratosphere. It

may open a new channel of understanding of photoreactivity on grains in interstellar space as well.

Acknowledgements

We wish to thank Yigal Lilach for his valuable help in performing this study. This research was partially supported by a grant from the German–Israel Foundation, US–Israel Binational Science Foundation and the Israel Science Foundation. The Farkas Center is supported by the Bundesministerium für Forschung und Technologie and the Minerva Gesellschaft für die Forschung mbh.

References

1 X. L. Zhou, X. Y. Zhu and M. J. White, *Surf. Sci. Rep.*, 1991, **13**, 73.
2 *Laser Spectroscopy and Photochemistry on Metal Surfaces, Part I and II*, ed. H.-L. Dai and W. Ho, World Scientific, New York, 1995.
3 M. Asscher, F. Zimmermann, L. Springsteen, P. L. Houston and W. Ho, *J. Chem. Phys.*, 1992, **96**(5), 4808–11.
4 J. D. Thrower, D. J. Burke, M. P. Collins, A. Dawes, P. D. Holtom, F. Jamme, P. Kendall, W. A. Brown, I. P. Clark, H. J. Fraser, M. R. S. McCoustra, N. J. Mason and A. W. Parker, *Astrophys. J.*, 2008, **673**, 1233.
5 M. P. Bernstein, S. A. Sandford, A. L. Mattioda and L. J. Allamandola, *Astrophys. J.*, 2007, **664**, 1264.
6 (*a*) M. S. Gudipati and L. J. Allamandola, *Astrophys. J.*, 2003, **596**, L198; (*b*) P. A. Gerakines, W. A. Schutte and P. Ehrenfreund, *Astron. Astrophys.*, 1996, **312**, 289 and references therein; (*c*) A. G. G. M. Tielens and L. J. Allamandola, in *Interstellar Processes*, ed. D. J. Hollenbach and H. A. Thronton, Riedel, Dordrecht, 1987.
7 T. Tachikawa, M. Fujitsuka and T. Majima, *J. Phys. Chem.*, 2007, **111**, 5259.
8 T. Livneh, L. Romm and M. Asscher, *Surf. Sci.*, 1996, **315**, 250.
9 R. S. Smith, C. Huang, E. K. L. Wong and B. D. Kay, *Phys. Rev. Lett.*, 1997, **79**, 909.
10 Y. Lilach and M. Asscher, *J. Chem. Phys.*, 2002, **117**, 6730.
11 R. Berger, Y. Lilach, Y. Ayoub and M. Asscher, *Isr. J. Chem.*, 2005, **45**, 97.
12 J. D. Thrower, D. J. Burke, M. P. Collins, A. Dawes, P. D. Holtom, F. Jamme, P. Kendall, W. A. Brown, I. P. Clark, H. J. Fraser, M. R. S. McCourstra, N. J. Mason and A. W. Parker, *Astrophys. J.*, 2008, **673**, 1233.
13 Y. Lilach and M. Asscher, *J. Chem. Phys.*, 2003, **119**, 407.
14 T. Livneh and M. Asscher, *J. Phys. Chem. B*, 2003, **107**, 11382.
15 John R. Barker, *Progress And Problems In Atmospheric Chemistry*, World Scientific, Singapore, 1996.
16 T. Livneh, Y. Lilach and M. Asscher, *J. Chem. Phys.*, 1999, **111**(24), 11138.
17 G. A. Kimmel, N. G. Petrik, Z. Dohnalek and B. D. Kay, *J. Chem. Phys.*, 2006, **125**, 044713.
18 R. S. Smith, C. Huang, E. K. L. Wong and B. Kay, *Surf. Sci.*, 1996, **376**, L13.
19 G. Held and D. Menzel, *Surf. Sci.*, 1994, **316**, 92.
20 The surface temperature jump due to pulsed laser heating is difficult to measure directly. However, indirect measurements and calculations based on absorption at the laser wavelength, heat conductivity and diffusivity of the substrate enable such estimates. See for example: Z. Rosenzweig and M. Asscher, *J. Chem. Phys.*, 1992, **96**(5), 4040–43 and references therein.
21 M. Menges, B. Baumeister, K. Al-Shamery, H.-J. Freund, C. Fischer and P. Andresen, *Surf. Sci.*, 1994, **316**, 103.
22 R. Zehr, A. Solodukhin, B. C. Haynie, C. French and I. Harrison, *J. Phys. Chem. B*, 2000, **104**, 3094.
23 Y. Lilach and M. Asscher, *J. Phys. Chem. B*, 2004, **108**, 4358–61 and references therein.